Heliyon 7 (2021) e08202

Contents lists available at ScienceDirect

Heliyon

journal homepage: www.cell.com/heliyon

Research article

Enhancement of hydrogen production using Ni catalysts supported by Gd-doped ceria

Opas Tojira [a], Jessica Gina Lomonaco [a], Thanathon Sesuk [b], Sumittra Charojrochkul [b], Pannipa Tepamatr [a,*]

[a] Department of Chemistry, Faculty of Science and Technology, Thammasat University, Pathumthani, Thailand
[b] National Energy Technology Center, NSTDA, Pathumthani, Thailand

ARTICLE INFO

Keywords:
Re
Ni
GDC
Hydrogen production
Water gas shift

ABSTRACT

A redox cycle between Ce^{4+} and Ce^{3+} is an elementary step in water gas shift (WGS) mechanism. By facilitating the redox cycle between +4 and +3 of cerium, a formation of oxygen vacancy can be enhanced. It is considered to be a dominating factor in developing the WGS performance and the stability of ceria in this work. We have facilitated the redox cycle in CeO_2 to enrich the WGS activity. The WGS reaction was carried out on Ni catalyst supported by Gd-doped ceria (GDC) from Daiichi. Ni and Re were added onto GDC by impregnation method to examine the role of Re addition on surface, structural and reducibility, which affected upon their catalytic activities. Rhenium has an influence on increasing the water gas shift performance of Ni/GDC catalysts because it facilitates the redox process at the surface of ceria, disperses Ni particles and enhances oxygen vacancy formation. The results indicate that the water gas shift activity of 1%Re4%Ni/GDC is higher than that of 5%Ni/GDC. The dispersion of active site on the surface of catalyst results in an increase of CO molecule adsorption and acceleration of the redox cycle between Ce^{4+} and Ce^{3+} of ceria support via oxygen vacancy generation. Therefore, using a combination of these two effects can enhance the WGS performance.

1. Introduction

Many chemical industries and the fuel cell industry utilize hydrogen to provide a pollution-free combustion and high energy density [1, 2, 3]. Hydrogen is a promising fuel for mobile and residential fuel cells. It is a sustainable fuel resource and emission free during the hydrogen reaction. Hence, hydrogen has received a widespread attention to reduce our dependence on fossil fuel, which has created environmental pollution. Currently, a production of hydrogen by natural gas steam reforming is still the predominant way in major industries [4]. Reforming process generates a synthesis gas, which contains H_2 and CO. However, CO must be eliminated because it deactivates Pt electrode in a low-temperature fuel cell. Therefore, a water gas shift (WGS) reaction has been applied to obtain hydrogen rich gas reformates.

Ceria based materials are widely used for many applications because of its high oxygen storage capacity and good reducibility [5, 6, 7, 8]. Excellent redox property of ceria provides an increase in the oxygen transport ability at ceria surface. In addition, a strong interaction between ceria support with active metal particles results in enhancing the metal dispersion and preventing the ceria support agglomeration. Oxygen vacancies within the catalyst can be introduced from the redox cycle between Ce^{4+} and Ce^{3+} of ceria [9, 10, 11, 12]. This provides sites for hydrogen dissociation, which is the rate-limiting step for water gas shift reaction. Therefore, increasing oxygen vacancy is a key factor in enhancing the water gas shift activity of CeO_2 based catalysts. Many researchers have tried to increase the oxygen vacancies in ceria-based materials to enrich the WGS activity. An addition of Zr to ceria was found to enhance the surface area, redox property and amount of oxygen vacancies [13, 14]. Some previous study revealed that Nd and La showed positive impact on Cu dispersion, redox properties and oxygen vacancy formation in Cu/CeO_2 catalysts [15]. Furthermore, it was found that an addition of Ba could enhance the sintering resistance, metal dispersion and the oxygen vacancy of ceria materials [16].

In this work, we have focused on accelerating the redox cycle between Ce^{4+} and Ce^{3+} of ceria for the bimetallic ReNi catalyst on Gd-doped ceria support to enhance the oxygen vacancies. The oxygen vacancy is the main factor to facilitate the redox cycle. In addition, an increase of the active metal of supported Ni catalysts alerts CO adsorption on the catalyst

* Corresponding author.
E-mail address: p.tepamat@gmail.com (P. Tepamatr).

https://doi.org/10.1016/j.heliyon.2021.e08202
Received 11 July 2021; Received in revised form 31 August 2021; Accepted 14 October 2021

surface, which leads to increasing rate of WGS reaction. Effects of rhenium addition on CeO_2 structure and reducibility were investigated using BET surface area, X-ray diffraction, H_2-temperature programmed reduction, chemisorption and X-ray photoelectron spectroscopy analyses to explain the relationship between the predominant factors (i.e. metal dispersion, metal area, and reducibility) and water gas shift activity.

2. Experimental procedure

2.1. Catalysts preparation

Impregnation method was used to prepare Ni/GDC catalyst. Nickel (II) nitrate hexahydrate (Alfa Aesar) was dissolved in a minimal amount of deionized (DI) water. The metal nitrate solution was added to 10% gadolinium doped ceria support (supplied by Daiichi).

NiRe/GDC catalyst was prepared using co-impregnation method. $Ni(NO_3)_2.6H_2O$ (Alfa Aesar) and NH_4ReO_4 (Sigma-Aldrich) were dissolved with DI water. The mixture solution of metal nitrate was added to GDC support (Daiichi). All samples were dried at 110 °C for 12 h and calcined at 650 °C for 8 h.

2.2. Catalyst characterization

The BET surface area of the specimens was performed using Quantachrome NOVA 1200e. Prior to the measurement, the catalysts were heated under vacuum at 300 °C for 6 h. The BET surface areas of all catalysts were estimated by using N_2 adsorption-desorption isotherms at 77 K in the relative pressure range of 0.05–0.3.

The X'Pert Pro diffractometer (PANalytical) operating at 0.02° step and 0.5 s per step over a 2θ range of 20–80° with the current of 40 mA and 40 kV was employed for X-ray powder diffraction measurements. The X-ray diffractograms were collected using nickel-filtered Cu K_α radiation. The full width at half maximum of the strongest (111) reflection was considered for the calculation of ceria crystallite size using Scherrer's equation.

A catalyst analyzer BELCAT-B was used for H_2-Temperature Programmed Reduction (H_2-TPR) experiment. The samples were treated under high purity He at 120 °C for 30 min prior to a TPR measurement. A mixed gas of 5%H_2–Ar was employed for TPR experiments operating from 50 °C to 1000 °C at the rate of 10 °C min^{-1}. The H_2 consumption during the reduction was determined using a thermal conductivity detector (TCD).

A mixed gas of 10%CO–He was introduced to the specimen for the measurement of the metal surface area from the total gas chemisorption. The metal surface area and the weight of the specimen were used for the calculation of metal dispersion. All specimens were reduced with H_2 at 400 °C for an hour. After cooling with He, carbon monoxide chemisorption pulse was analysed under the flow of carbon monoxide in helium carrier gas at 50 °C at the rate of 30 ml min^{-1}. The flow of carbon monoxide out of the reactor was monitored using a TCD.

Amount of adsorption per 1 g of sample V_m in cm^3g^{-1}

$$V_m = V_{chem}/m \quad (1)$$

Metal dispersion (percentage of metal surface exposure) D (%)

$$D = V_{chem}/26519 \times SF \times MW \times 100/c \quad (2)$$

where V_m is an amount of adsorption in cm^3, m is the weight of specimen in g, MW is the atomic weight of metal in g mol^{-1}, and SF is the stoichiometry factor.

Metal weight (c) in g:

$$c = m \times p/100 \quad (3)$$

A_m is metal surface area (surface area of metal per 1 g of sample) in m^2g^{-1}

$$Am = V_{chem}/26519 \times SF \times 6.02 \times 10^{23} \times 10^{-18}/m \quad (4)$$

where p is the weight percentage of supported metal content in wt%, and σ_m is the crossectioned area of a metal in atom/nm^2.

The Raman spectra of Ni and NiRe catalysts were performed using Perkin Elmer System 2000 FT-IR/FT-Raman. The spectra were collected using Ar ion laser irradiation in the range of 200–2000 cm^{-1} with an output power of 10 mW and wavelength of 532 nm.

The chemical composition of specimen surface was investigated using an X-ray photoelectron spectrometer (XPS, AXIS ULTRA DLD, Kratos analytical). The catalysts were reduced ex-situ under a flow of 5%H_2/N_2 at 400 °C for 1 h before the analysis. The base pressure in the XPS analysis chamber was about 5×10^{-9} torr. The specimens were excited with X-ray hybrid mode of 700 × 300 μm spot area with a monochromatic Al $K\alpha_{1,2}$ radiation at 1.4 keV. X-ray anode runs at 15kV 10mA 150 W. The photoelectrons are detected with a hemispherical analyzer positioned at an angle of 90° with respect to the normal to the sample surface. The spectra are calibrated using the C1s line (BE = 285 eV).

2.3. Water gas shift activity

Water gas shift performance was tested using a fixed bed reactor with 4 mm inner diameter. The catalysts (~150 mg) were loaded into a stainless steel tube reactor between two layers of quartz wool. The reactor was placed inside a tube furnace. Prior to the water gas shift activity measurement, the prepared catalyst was reduced by heating in 5% H_2/N_2 balanced gas from room temperature to 400 °C and held for 1 h. After reducing the catalyst, the temperature was lowered to 100 °C. Activity test of Ni catalysts was performed in the temperature range of 100–500 °C. H_2O was fed through a pre-heater using a syringe pump. The feed gas contained 5% CO, 10% H_2O and 85% N_2. Preliminary measurements were operated to consider proper conditions from which internal and external mass transfer effects were not dominant. When considering the effect of external mass transfer, the particle size diameter of the catalysts was between 100-200 μm in all conditions. Furthermore, the total flow rate was kept constant at 100 ml min^{-1} in all experiments. The outlet gasses were analysed using an on-line Shimadzu GC-14B gas chromatography equipped with TCD. The column utilized in the gas chromatography was a Unibead C. The WGS activities were calculated using Eq. (5):

$$\%CO\ conversion = \frac{CO_{in} - CO_{out}}{CO_{in}} \times 100 \quad (5)$$

The WGS rates were tested in separate experiments using 20 mg of catalysts and the feed gas mixture of 5% CO, 10% H_2O and 85% N_2 where the CO conversion was less than 30%.

$$Rate = (F \times X)/m \quad (6)$$

where Rate is the WGS rate (mol g^{-1} s^{-1}), F is the molar flow rate of CO (mol s^{-1}), m is the weight of the samples (g), and X is the carbon monoxide conversion.

3. Results and discussion

3.1. Standard characterization of Ni catalysts

Figure 1 presents X-ray diffraction patterns of Ni catalysts. XRD spectra of all catalysts correspond to ceria in fluorite-type cubic crystal structure. The lattice constant of ceria in the catalysts was calculated from 111 diffraction peak broadening. The ceria lattice parameters of GDC (Daiichi) and Ni catalysts were found in the range of 0.5421–0.5424 nm. Nickel and rhenium ion could not be inserted into the lattice of CeO_2 due to the nature of impregnation synthesis. There are two diffraction peaks at $2\theta = 37.3^o$ and 43.4^o which correspond to NiO in supported Ni catalysts. The NiO diffraction peaks are very weak suggesting that there is

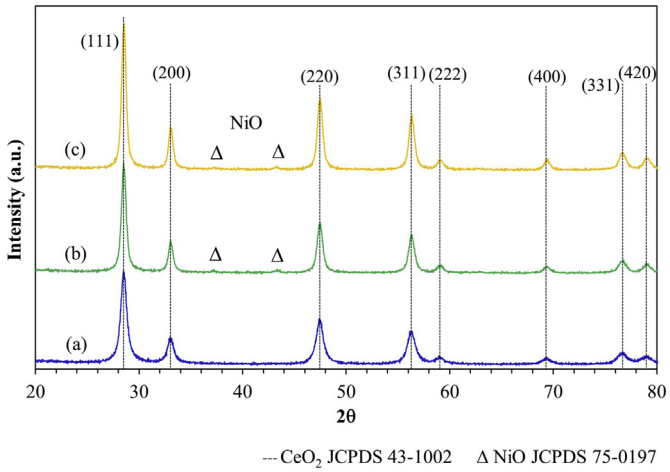

Figure 1. XRD patterns of supported Ni catalysts, (a) GDC, (b) 5%Ni/GDC and (c) 1%Re5%Ni/GDC.

very small amount of NiO. The results of BET surface areas and crystallite size are summarized in Table 1. An addition of nickel and rhenium onto GDC (Daiichi) by impregnation method leads to an increase in crystallite size and a reduction of the surface area. This result is probably due to CeO_2 crystallites agglomeration after calcination at high temperature. CO chemisorption analysis was operated to study a dispersion of nickel over Ni/GDC materials. The reduced ceria gives some signals to the CO titration. Indeed, Ce^{3+} species can also react with CO during the investigation. Thus, the CO-chemisorption was measured on doped ceria without an addition of nickel, used as a blank test. From the results of chemisorption analysis shown in Table 1, it is found that an addition of rhenium to Ni/GDC (Daiichi) enhances a dispersion of Ni metal on the GDC support. Metallic Ni was believed to provide active sites for the WGS reaction [17]. The effect of Re addition on metallic Ni surface area was probed, which revealed that ReNi/GDC catalyst had the highest metallic surface area of 42 m^2/g. Generally, catalysts with higher metallic surface area provide an increase in catalytic activity, as more of their surface active sites are exposed to reactants [18, 19].

3.2. H_2-TPR of Ni catalysts

TPR profiles of Ni catalysts are shown in Figure 2. The reduction peaks of GDC support appear at 510 °C and 800 °C, which are assigned to the reduction of surface and the bulk CeO_2, respectively. TPR profile of 1%Re/GDC is also plotted for a comparison. The reduction of Rhenium oxide occurs at high temperature (about 400 °C), which indicates that rhenium species alone is difficult to reduce. On the contrary, a combination of Ni and Re species enhances their reducibility. For Ni/GDC, there are three reduction peaks corresponding to the reduction of nickel oxide, surface region of CeO_2 and the bulk. An addition of Ni onto Gd-doped ceria from Daiichi shifts the surface reduction toward lower temperatures. H_2-TPR profile of bimetallic NiRe on Gd-doped ceria from

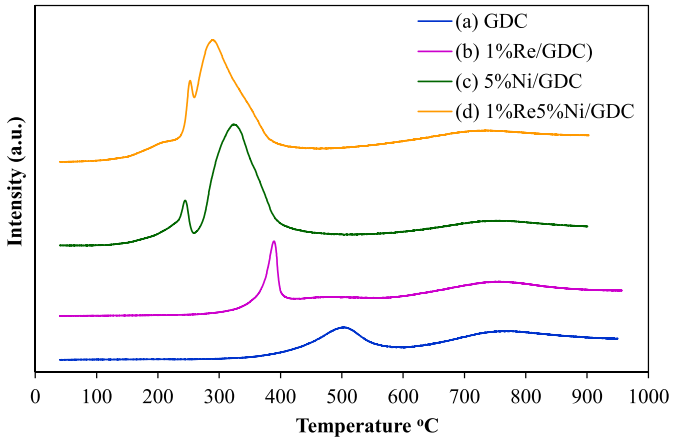

Figure 2. H_2-TPR profiles of supported Ni catalysts, (a) GDC, (b) 1%Re/GDC, (c) 5%Ni/GDC and (d) 1%Re5%Ni/GDC.

Daiichi is also compared. It is clearly seen that Re addition onto Ni/GDC drastically shifts the reduction peak of surface oxygen to lower temperature. From the comparison between Ni/GDC and ReNi/GDC catalysts, it was found that an addition of Re increased H_2 consumption (Table 2), indicating an improvement of reducibility of Ni catalyst. These results imply that rhenium helps Ni in reducing ceria and leads to the enrichment of Ce^{3+} at the ceria surface, which gives rise to oxygen vacancies. This simplifies the electron movement at the surface, hence, enhancing easier surface reduction [11].

3.3. Raman spectroscopy

Defect structures of supported Ni catalysts were investigated using Raman spectroscopy. Figure 3 illustrates the Raman spectra of NiRe/GDC, Ni/GDC and GDC support. A Raman peak at ~460 cm^{-1} is the symmetrical stretching of the oxygen atoms around Ce ions (F_{2g} mode) of the cubic fluorite crystal structure of CeO_2. The intensity of this peak decreases when addition of Ni or NiRe onto GDC support. This is due to high metal dispersion at the surface. In addition, there is another broad peak of NiRe/GDC and Ni/GDC starting from 520 to 650 cm^{-1}. It is a defect-induced mode band, which is due to the presence of surface

Table 2. WGS rate and H_2 consumption of Ni-based catalysts.

Catalyst	Rate at 350 °C	E_a	H_2-TPR	
	(mmol/kg.s)	(kJ/mol)	Peak position (°C)	H_2 consumption (mmol/g)
5%Ni/GDC	58	69 ± 0.6	240, 321	1.26, 16.41
1%Re5% Ni/GDC	77	58 ± 0.4	205, 244, 280	0.66, 0.74, 16.47

Table 1. Surface areas, crystallite size and %dispersion of Ni catalysts.

Catalysts	S_{BET}[a]	Crystallite[b]	Lattice[b]	%dispersion[c]	S_{Ni}[c]	Average particle
	(m^2/g)	size (nm)	parameter (nm)		(m^2_{Ni}/g_{Ni})	size[c] (nm)
GDC	76	12.0	0.5424	1.8	-	-
5%Ni/GDC	45	15.1	0.5423	4.9	32.5	20.7
1%Re5%Ni/GDC	42	16.1	0.5421	6.5	42.0	14.9

[a] Estimated from N_2 adsorption at −196 °C.
[b] Calculated from 111 diffraction peak broadening.
[c] Estimated from CO-chemisorption.

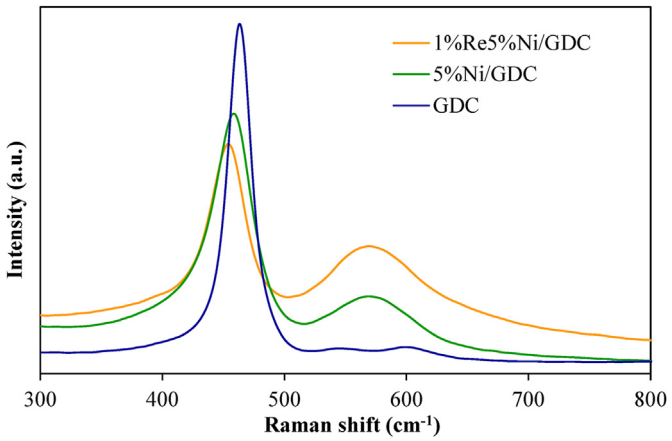

Figure 3. Raman spectra of supported Ni catalysts.

defects or a different charge state of doping cations [20]. These defects are related to the evolution of oxygen vacancies.

3.4. XPS analysis

The relationship between chemical species on the surface region of the catalysts and reducibility were studied using XPS analysis. The results are summarized in Table 3. The Ni $2p_{3/2}$ XPS spectra of Ni/GDC and ReNi/GDC catalysts were deconvoluted as shown in Figure 4. The prepared catalyst was reduced under a flow of 5%H_2/N_2 at 400 °C for 1 h before performing the XPS analysis. After the reduction, Ni was in the metallic state whereas the different nickel species co-existed due to the interaction with GDC. The peak around 853 eV is attributed to Ni^0 whereas the following two peaks at higher binding energy are assigned to surface Ni^{2+} [21]. Their relative ratios are summarized in Table 3. Ni^0 was suggested to be the dominant active species in accelerating the reactants [22]. For Re addition onto Ni/GDC, it was found that XPS spectrum of surface Ni^{2+} shift to lower Ni binding energy values (856.35), which indicates that Re appears to hinder the strong interaction between Ni and GDC. Thus, metallic nickel formation is favored [23]. The enhancement of Ni^0 content of ReNi/GDC implies a superior WGS activity of Ni catalyst with Re addition.

3.5. WGS activity of Ni catalysts

Figure 5 shows the WGS activity of Ni catalysts. The WGS activity of GDC (Daiichi) support was also plotted for a comparison. It was found that 5%Ni/GDC (Daiichi) is an active catalyst for a water gas shift reaction. The activity of 5%Ni/GDC (Daiichi) starts at about 200 °C and ascends to reach the maximum of 95% conversion at 350 °C. The conversion above 350 °C reaches equilibrium and then slightly decreases. Moreover, it can be seen that ReNi/GDC exhibits higher CO conversion rate compared to 5%Ni/GDC catalysts. The bimetallic catalyst ReNi/GDC becomes active above 200 °C and reaches the maximum of 99% conversion rapidly at around 350 °C. The combination of H_2-TPR and CO chemisorption results suggests that ReNi/GDC has an excellent redox property, the smallest particle size and the highest nickel dispersion on GDC support, which contributes to the highest water gas shift activity [24, 25]. 1%Re5%Ni/GDC (Daiichi) was further examined at 270 °C for 24 h. The CO conversion versus time plot is presented in Figure 6. The water gas shift activity of ReNi/GDC was kept constant for the whole 24 h period. Therefore, this catalyst is more resistant towards deactivation than Ni/GDC. In addition, the apparent activation energy (E_a) was estimated from the slope of the Arrhenius plot in the temperature range of 200–400 °C (see Figure 7). The estimated parameters are shown in Table 2. In comparison with the values obtained from the literature, it is rather difficult to draw a conclusion due to the fact that most studies were

Table 3. XPS analysis for quantitative measurement of Ni-based catalysts.

Catalyst	BE Ni $2p_{3/2}$ (eV)	Ni^0 (%)
5%Ni/GDC	853.07	28.2
	854.92	
	856.62	
1%Re5%Ni/GDC	853.11	34.1
	854.91	
	856.35	

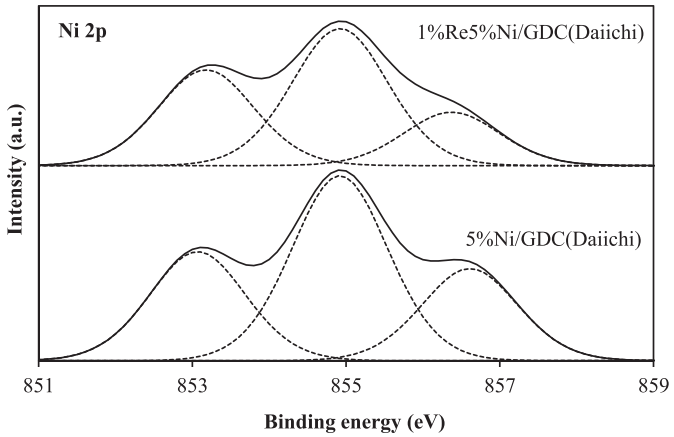

Figure 4. XPS spectra of supported Ni catalysts for Ni 2p.

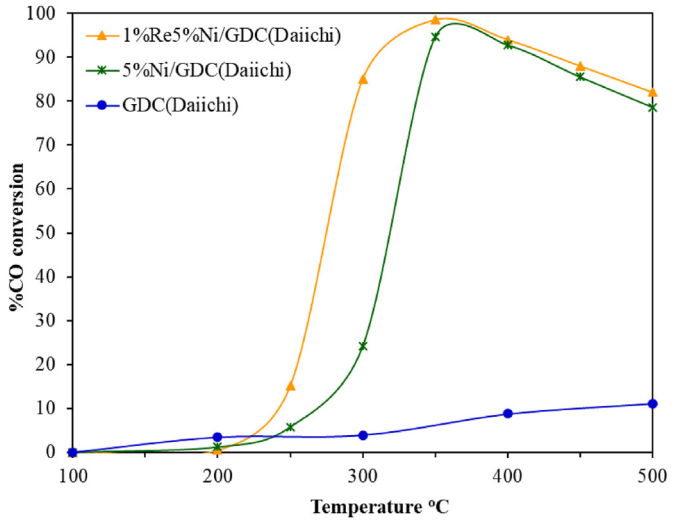

Figure 5. WGS catalytic activity of supported Ni catalysts.

carried out under different conditions and the inhibitory effect of CO_2 and H_2 on the forward reaction rate was not mentioned. Generally, the activation energies reported are in the range of 60–80 kJ mol^{-1} for transition metal catalysis supported on ceria [22]. The values are consistent with the apparent E_a value obtained from this study (58 kJ/mol for 1%Re5%Ni/GDC and 69 kJ/mol for 5%Ni/GDC).

4. Conclusions

The role of Re on the water gas shift activity was investigated. The best activities were found for ReNi on GDC from Daiichi. The catalytic activity of ReNi/GDC (Daiichi) rapidly increased to attain the maximum of 99% conversion at 350 °C. An addition of Re into Ni/GDC provided a high metal

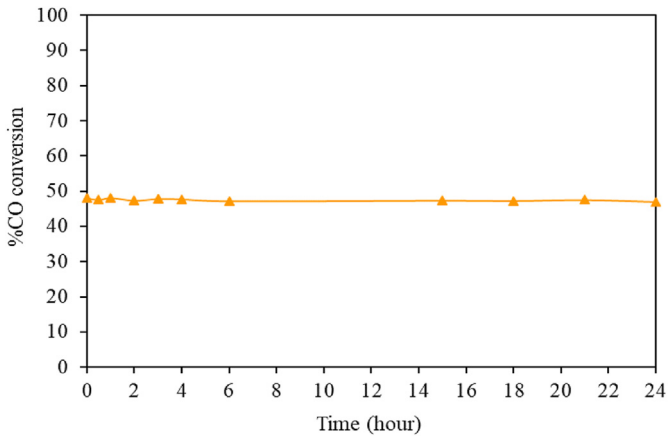

Figure 6. Stability of 1%Re5%Ni/GDC (Daiichi) at 270 °C.

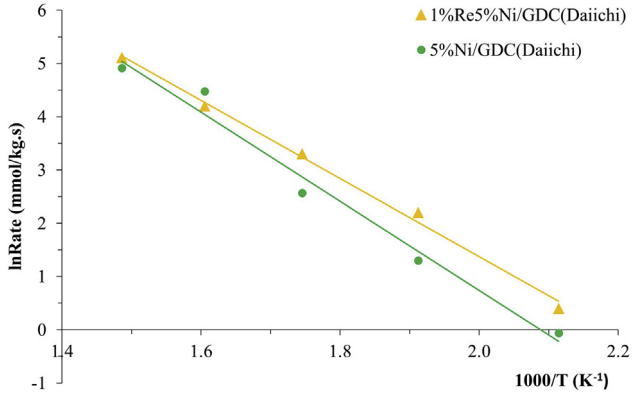

Figure 7. Arrhenius plot of reaction rate over Ni catalysts.

surface area and a small particle size. Excellent physicochemical properties of ReNi/GDC strongly affected Ni dispersion and reducibility of Ni catalyst prepared by impregnation method. This ability helped to facilitate the redox cycle of the WGS reaction, resulting in a high reduction of ceria with Ni. ReNi/GDC exhibited higher CO conversion than Ni/GDC. The high WGS activity of ReNi/GDC was mainly related to enhanced reducibility and the active Ni^0 species. An increase of the surface area of metallic Ni improved the reactant CO adsorption and enhanced the water gas shift rate. It is concluded that ReNi/GDC is a promising catalyst for a hydrogen production application by water gas shift reaction.

Declarations

Author contribution statement

Opas Tojira: Analyzed and interpreted the data; Wrote the paper.

Jessica Gina Lomonaco: Performed the experiments.

Thanathon Sesuk: Performed the experiments; Contributed reagents, materials, analysis tools or data.

Sumittra Charojrochkul: Analyzed and interpreted the data; Contributed reagents, materials, analysis tools or data; Wrote the paper.

Pannipa Tepamatr: Conceived and designed the experiments; Performed the experiments; Analyzed and interpreted the data; Contributed reagents, materials, analysis tools or data; Wrote the paper.

Funding statement

This work was supported by the Faculty of Science and Technology, Thammasat University, Contract No. SciGR26/2563. The Thammasat University Research Unit in smart materials from biomass. and Thailand Graduate Institute of Science and Technology (TGIST), Contract No. SCA-CO-2021-14622-TH.

Data availability statement

Data will be made available on request.

Declaration of interests statement

The authors declare no conflict of interest.

Additional information

No additional information is available for this paper.

Acknowledgements

The authors are thankful to Prof. S. Seraphin (Profession Authorship Center, Thailand National Science and Technology Development Agency) for invaluable comments in manuscript revision.

References

[1] C. Chen, Y. Zhan, D. Li, Y. Zhang, X. Lin, L. Jiang, et al., Preparation of CuO/CeO2 catalyst with enhanced catalytic performance for water-gas shift reaction in hydrogen production, Energy Technol 6 (2018) 1096–1103.

[2] H.S. Na, D.W. Jeong, W.J. Jang, J.O. Shim, H.S. Roh, The effect of preparation method on Fe/Al/Cu oxide-based catalyst performance for high temperature water gas shift reaction using simulated waste-derived synthesis gas, Int. J. Hydrogen Energy 40 (2015) 12268–12274.

[3] J.O. Shim, H.S. Na, S.Y. Ahn, K.W. Jeon, W.J. Jang, B.H. Jeon, et al., An important parameter for synthesis of Al_2O_3 supported Cu-Zn catalysts in low-temperature water-gas shift reaction under practical reaction condition, Int. J. Hydrogen Energy 44 (2019) 14853–14860.

[4] M. Soria, C. Rocha, S. Tosti, A. Mendes, L.M. Madeira, COx free hydrogen production through water-gas shift reaction in different hybrid multifunctional reactors, Chem. Eng. J. 356 (2018) 727–736.

[5] A. Uzunoglu, D.A. Kose, L.A. Stanciu, Synthesis of CeO2-based core/shell nanoparticles with high oxygen storage capacity, Int. Nano Lett. 7 (2017) 187–193.

[6] J. Zhang, H. Kumagai, K. Yamamura, S. Ohara, S. Takami, A. Morikawa, H. Shinjoh, K. Kaneko, T. Adschiri, A. Suda, Extra-low-temperature oxygen storage capacity of CeO_2 nanocrystals with cubic facets, Nano Lett 11 (2011) 361–364.

[7] T. Montini, M. Melchionna, M. Monai, P. Fornasiero, Fundamentals and catalytic applications of CeO_2-based materials, Chem. Rev. 116 (2016) 5987–6041.

[8] P. Tepamatr, N. Laosiripojana, T. Sesuk, S. Charojrochkul, Effect of samarium and praseodymium addition on water gas shift performance of Co/CeO_2 catalysts, J. Rare Earths 38 (2020) 1201–1206.

[9] S. Sangsong, T. Ratana, S. Tungkamani, T. Sornchamni, M. Phongaksorn, Effect of CeO_2 loading of the Ce-Al mixed oxide on ultrahigh temperature water-gas shift performance over Ce-Al mixed oxide supported Ni catalysts, Fuel 252 (2019) 488–495.

[10] R. Farra, M. Garcúía-Melchor, M. Eichelbaum, M. Hashagen, W. Frandsen, J. Allan, et al., Promoted ceria: a structural, catalytic, and computational study, ACS Catal 3 (2013) 2256–2268.

[11] P. Tepamatr, N. Laosiripojana, S. Charojrochkul, Water gas shift reaction over monometallic and bimetallic catalysts supported by mixed oxide materials, Appl. Catal. Gen. 523 (2016) 255–262.

[12] P. Tepamatr, E. Buarod, N. Laosiripojana, S. Charojrochkul, Study of water gas shift reaction over ceria based catalysts in solid oxide fuel cells, ECS Trans 68 (2015) 1207–1217.

[13] D.W. Jeong, H.S. Na, J.O. Shim, W.J. Jang, H.S. Roh, A crucial role for the CeO_2–ZrO_2 support for the low temperature water gas shift reaction over Cu–CeO2–ZrO_2 catalysts, Catal. Sci. Technol. 5 (2015) 3706–3713.

[14] D.W. Jeong, W.J. Jang, H.S. Na, J.O. Shim, A. Jha, H.S. Roh, Comparative study on cubic and tetragonal Cu–CeO_2–ZrO_2 catalysts for water gas shift reaction, J. Ind. Eng. Chem. 27 (2015) 35–39.

[15] Y. She, Q. Zheng, L. Li, Y. Zhan, C. Chen, Y. Zheng, et al., Rare earth oxide modified CuO/CeO_2 catalysts for the water-gas shift reaction, Int. J. Hydrogen Energy 34 (2009) 8929–8936.

[16] Y.L. Lee, K.J. Kim, W.J. Jang, J.O. Shim, K.W. Jeon, H.S. Na, et al., Increase in stability of BaCo/CeO_2 catalyst by optimizing the loading amount of Ba promoter for high-temperature water-gas shift reaction using waste-derived synthesis gas, Renew. Energy 145 (2020) 2715–2722.

[17] Y. Yu, Z. Bian, Z. Wang, J. Wang, W. Tan, Q. Zhong, S. Kawi, CO_2 methanation on Ni-Ce0.8M0.2O2 (M=Zr, Sn or Ti) catalyst: suppression of CO via formation of bridging carbonyls on nickel, Catal. Today (2020).

[18] Y.L. Lee, A. Jha, W.J. Jang, J.O. Shim, K.W. Jeon, H.S. Na, H.M. Kim, D.W. Lee, S.Y. Yoo, B.H. Jeon, J.W. Bae, H.S. Roh, Optimization of cobalt loading in Co–CeO2

catalyst for the high temperature water–gas shift reaction, Top. Catal. 60 (9–11) (2017) 721–726.

[19] U. Izquierdo, V.L. Barrio, J.F. Cambra, J. Requies, M.B. Güemez, P.L. Arias, et al., Hydrogen production from methane and natural gas steam reforming in conventional and microreactor reaction systems, Int. J. Hydrogen Energy 37 (2012) 7026–7033.

[20] J. Tan, D. Lee, J. Ahn, B. Kim, J. Kim, J. Moon, Thermally driven *in situ* exsolution of Ni nanoparticles from (Ni, Gd)CeO_2 for high-performance solid oxide fuel cells, J. Mater. Chem. 6 (37) (2018) 18133–18142.

[21] J.P. Bortolozzi, T. Weiss, L.B. Gutierrez, M.A. Ulla, Comparison of Ni and Ni-Ce/Al_2O_3 catalysts in granulated and structured forms: their possible use in the oxidative dehydrogenation of ethane reaction, Chem. Eng. J. 246 (2014) 343–352.

[22] L. Liu, Q. Wang, J. Song, S. Ahmad, X. Yang, Y. Sun, Plasma-assisted catalytic reforming of toluene to hydrogen rich syngas, Catal. Sci. Technol. 7 (2017) 4216–4231.

[23] S.D. Senanayake, J.A. Rodriguez, D. Stacchiola, Electronic metal−support interactions and the production of hydrogen through the water-gas shift reaction and ethanol steam reforming: fundamental studies with well-defined model catalysts, Top. Catal. 56 (2013) 1488–1498.

[24] E. Pablo Giunta, P. Giunta, G. Baronetti, F. Mariño, Cu and/or Ni catalysts over CePr oxide for the water gas shift reaction: an experimental study, kinetic fitting and reactor simulation, React. Kinet. Mech. Catal. 121 (2017) 607–628.

[25] Z. Zhang, L. Liu, B. Shen, C. Wu, Preparation, modification and development of Ni-based catalysts for catalytic reforming of tar produced from biomass gasification, Renew. Sustain. Energy Rev. 94 (2018) 1086–1109.